Journal of Animal & Plant Sciences, 34(4): 2024, Page: 999-1011
ISSN (print): 1018-7081; ISSN (online): 2309-8694
https://doi.org/10.36899/JAPS.2024.4.0782

HYDROALCOHOLIC EXTRACT OF *Lepidium draba* L. AMELIORATES CAPECITABINE -INDUCED ENTEROCOLITIS IN RATS

P. Xiao[1], H. Ma[2], C. Kuang[3]and W. Wang[1*]
[1]Department of Gastroenterology, Xi'an GAOXIN Hospital, Xi'an, China, 710000.
[2]Department of General Medicine, Zhumadian Central, Ral Hospital, Zhumadian, Henan, 463000, China.
[3]Department of General Surgery, Gaoyou people's hospital, Yangzhou, 225600, China.
Corresponding author's email: wwj18700796618@sina.com
https://orcid.org/0009-0002-4383-9845.

ABSTRACT

This study investigated the protective properties of *Lepidium draba* L. hydroalcoholic extract (LDHE) against enterocolitis induced by Capecitabine (CT), utilizing biochemical, molecular, and histopathological analyses. A study was conducted involving 50 Wistar rats divided into 5 groups of ten rats over 60 days: healthy, 400 mg/kg LDHE, 20 mg/kg CT, and two co-treatment groups receiving both CT and 200 and 400 mg/kg LDHE groups. On the 61st day, serum nitric oxide, antidiuretic hormone (ADH), arginine vasopressin (AVP), tumor necrosis factor-α, interleukin-6, chemokine C-X-C motif ligand 1 (CXCL-1), and interleukin-1β levels were measured, along with the activity of glutathione peroxidase, catalase, and superoxide dismutase enzymes. To evaluate tissue oxidative stress in the intestine, measurements were taken for FRAP, thiol, and TBARS levels. Apoptosis in the intestine was assessed by examining the Bax/Bcl-2, caspase-3, and p53 expression via real-time PCR. Furthermore, real-time PCR was employed to evaluate water homeostasis by examining the AQP3, AQP8, and AQP10 expression, while protein expression was analyzed using western blotting. LDHE extract effectively regulates inflammatory cytokine levels and modulates ADH and AVP levels, thereby preserving serum and intestinal osmotic balance. Furthermore, it attenuated the Bax/Bcl-2, caspase-3, and p53 mitochondrial apoptotic pathways while enhancing the expression of AQP3, AQP8, and AQP10 genes in intestinal tissue. The study suggests that LDHE holds promise in the treatment of enterocolitis in chemotherapy patients.

Keywords: *Lepidium draba* L., Capecitabine, Intestine, Enterocolitis, Apoptosis, Aquaporins

Published first online June 13, 2024 Published final August 25, 2024

INTRODUCTION

Chemotherapy-induced enterocolitis (CIE) represents a well-documented complication that may arise as an adverse effect of cancer therapy. Nonetheless, several pivotal processes have been discerned as contributors to CIE's pathogenesis (Wang *et al*., 2021a). Chemotherapy agents exert diverse detrimental impacts on the intestinal milieu. They directly assail intestinal epithelial cells, compromising the integrity of the intestinal barrier. This breach escalates permeability, facilitating the ingress of bacteria and toxins into intestinal tissues. Subsequently, the compromised tissue incites an inflammatory cascade typified by immune cell activation and the liberation of pro-inflammatory cytokines and chemokines (Shakir *et al*., 2019). This immune dysregulation perpetuates tissue damage and sustains the inflammatory milieu. Additionally, chemotherapy instigates oxidative stress by perturbing the equilibrium between reactive oxygen species (ROS) production. This imbalanced ROS generation engenders oxidative harm to cellular constituents, exacerbating tissue injury and inflammation (Zhao *et al*., 2022). CIE correlates with an aberration in immune tolerance mechanisms within the intestines, instigating an abnormal immune response against intestinal tissue, thereby intensifying inflammation and tissue devastation (Reyna-Figueroa *et al*., 2019). Chemotherapy medications have been observed to impede and diminish the expression of intestinal aquaporins (AQPs). AQPs represent a family of membrane proteins crucial for regulating water transport across cell membranes, including those within the intestines. Recent findings indicate the involvement of AQPs in the onset of CIE. Disruption of AQP function leads to disturbances in water homeostasis and compromises intestinal barrier integrity (Kamar *et al*., 2020). Any alterations in AQP expression or function can impede the regenerative potential of intestinal epithelial cells, hindering the healing cascade in CIE (Zhu *et al*., 2017).

Besides exerting apoptotic effects on tumor cells, chemotherapy drugs also induce distinct apoptotic pathways in normal host cells, including intestinal cells. Studies suggest that chemotherapy drugs stimulate apoptosis in intestinal cells by enhancing the expression of caspase-9 and apoptotic protease-activating factor 1 (Apaf-1) (van den Boogaard *et al*., 2022). Furthermore, these drugs elevate p27 levels, causing cell cycle arrest and apoptosis in intestinal cells (Salaroglio *et al*., 2019). Consequently, these pathways lead to the phosphorylation and activation of downstream targets, including transcription factors and apoptotic regulators like Bax and Bcl-2, thereby influencing intestinal cell apoptosis. Additionally, chemotherapy drugs have the potential to regulate the expression of cyclin D1, resulting in its downregulation. This disturbance in cell cycle progression further enhances apoptosis in intestinal cells (Wang *et al*., 2019).

Capecitabine (CT) is a widely used oral chemotherapy medication employed in the treatment of diverse cancer types, including breast, colorectal, and gastric cancers. It serves as a primary therapeutic option for metastatic breast cancer, colorectal cancer, and gastric cancer, frequently administered either as a frontline treatment or as adjuvant therapy (Masuda *et al*., 2017). CT can be utilized alone or in combination with other chemotherapy agents or targeted therapies. Common adverse effects associated with CT encompass gastrointestinal manifestations such as diarrhea, nausea, vomiting, and abdominal discomfort. Additionally, potential side effects may include fatigue, hand-foot syndrome (palmar-plantar erythrodysesthesia), stomatitis, dermatitis, myelosuppression (reduced blood cell counts), and heightened susceptibility to infections (Siddiqui *et al*., 2019). CT functions as a prodrug, undergoing conversion into its active form, fluorouracil (5-FU), within the body. The metabolites of 5-FU, including fluorouridine triphosphate (FUTP) and fluorodeoxyuridine monophosphate (FdUMP), integrate into RNA and DNA, respectively, disrupting their synthesis and inducing cytotoxic effects. The active metabolite 5-FU acts as an antimetabolite, impeding DNA and RNA synthesis, thereby interfering with their normal functions, disrupting cell division, and precipitating cell death. Moreover, 5-FU inhibits thymidylate synthase, an enzyme crucial for thymidine synthesis, a DNA building block. By thwarting thymidylate synthase activity, 5-FU diminishes thymidine availability for DNA synthesis, further impeding cell proliferation (Zhu *et al*., 2019). The precise mechanisms underlying CT-induced enterocolitis remain incompletely elucidated but likely entail a combination of immune dysregulation, oxidative stress, and direct toxic impacts on the intestinal mucosa. Studies have demonstrated that CT metabolites, notably 5-FU, can instigate various molecular pathways implicated in enterocolitis development, including the Bax/Bcl-2/p53 mitochondrial apoptosis pathway (Wang *et al*., 2019). Furthermore, CT inhibits the PI3K/Akt/mTOR signaling pathways, contributing to enterocolitis and intestinal inflammation (McRee *et al*., 2018; Inala and Pamidimukkala, 2023).

Lepidium draba L. (LDHE) is a deciduous plant species belonging to the Brassicaceae family. The compound and pinnate leaves of LDHE consist of multiple leaflets arranged oppositely along a central axis called a rachis, typically numbering between 7 to 13 leaflets. This tree species is indigenous to various regions of Europe, including the British Isles, as well as parts of Asia, commonly inhabiting deciduous forests, woodlands, and riverbanks. In traditional medicine, the leaves of LDHE have been utilized for diverse medicinal purposes. They are reputed to possess therapeutic properties effective in managing conditions such as diabetes, nausea, vomiting, digestive disorders, diarrhea, fatty liver, and various tumors, notably hepatocellular carcinoma and colon cancer (Ali *et al*., 2020). Liquid chromatography-electrospray ionization-mass spectrometry (LC-ESI-MS) analyses of LDHE extract have unveiled a significant presence of polyphenolic compounds, encompassing catechin, p-coumaric acid, isoquercitrin, daidzein, kaempferol, scopoletin, caffeic acid, genistein, and quercetin. These polyphenolic compounds, renowned for their anti-inflammatory, antioxidant, and immunomodulatory properties, have been investigated for their potential in mitigating enterocolitis (Ouissem *et al*., 2018; Tóth *et al*., 2017). The objective of our study was to investigate the potential protective and therapeutic effects of LDHE against CT-induced enterocolitis (CIE) in rats. We employed biochemical, molecular, and histopathological methodologies to evaluate the influence of LDHE on CT-induced enterocolitis.

MATERIALS AND METHODS

LDHE preparation: After collection and verification by a botanist, fresh leaves of LDHE weighing 5000 grams underwent drying at 37°C in a dark environment. Subsequently, a powder was obtained from the dried leaves using a soil grinder and combined with 70% ethanol/water (v/v). The mixture then underwent incubation at 35°C for 72 hours, followed by filtration through a paper filter. The filtrate was then concentrated using a rotary evaporator, yielding an extract weighing 300 grams. This extract was subsequently stored at 4°C for preservation (Jelodar *et al*., 2018).

Subjects and experimental design: Prior to commencing the study, a 72-hour acclimatization period was considered for animals to adjust to the experimental conditions. Rats displaying symptoms of illness, particularly digestive disturbances such as diarrhea and

anorexia, were excluded from the study. Adherence to international standard guidelines, protocols, and ethical regulations established by the relevant ethics committee was ensured throughout the experiment (ethics committee of Gaoyou People 's Hospital, approval number: 202409). The rats were kept under standard laboratory conditions at 25±3°C, with relative humidity at 45±4%, and a 12-hour dark/light cycle. They had access to standard rodent pellets and tap water.

Subsequently, a total of 50 adult male Wistar rats weighing between 180±20 grams were divided into 5 groups and observed for 60 days as follows:

1. Healthy group: Administered 1 ml of distilled water orally.
2. 400 LDHE group: Given 400 mg/kg of LDHE orally.
3. CT group: Administered 500 mg/kg of CT orally.
4. Co-treatment group 1 (CT + 200 LDHE): Received CT along with 200 mg/kg of LDHE orally.
5. Co-treatment group 2 (CT + 400 LDHE): Received CT along with 400 mg/kg of LDHE orally.

The LD_{50} technique, along with pilot studies and similar investigations involving CT and LDHE, was employed to determine the effective dose of non-toxic treatment. Throughout the study, CT and LDHE were administered daily at fixed intervals: CT at 9 am and LDHE at 3 pm (Wang *et al*., 2021a; Sakai *et al*., 2020).

LD_{50} of LDHE: The LD_{50} of LDHE was assessed using Lork's two-step method. Initially, 9 rats were assigned to 3 separate groups and received LDHE at doses of 25, 250, and 2500 mg/kg by gavage, with subsequent monitoring for potential mortality or toxic effects within a 24-hour period. Subsequently, another 3 rats in 3 separate groups received LDHE at doses of 50, 500, and 5000 mg/kg by gavage and were similarly monitored within 24 hours. The highest safe dose (D safe) and the lowest lethal dose (D toxic) identified during this observation period were then utilized in Lork's formula to determine the LD_{50} of LDHE, calculated as LD_{50} = (D safe × D toxic) 1/2.

Throughout the study duration, the survival rate was plotted using Kaplan-Meier curves (Wang *et al*., 2021b; Festing, 2006).

Arginine vasopressin (AVP) and antidiuretic hormone (ADH) serum levels: At the end of the study, following the euthanasia of the rats (via pre-anesthesia/anesthesia using 30 mg/kg ketamine 10% and 50 mg/kg xylazine 2%), blood samples were obtained from the heart, and serum specimens were subsequently separated using a centrifuge. Utilizing commercial ELISA kits, the serum levels of ADH and AVP were quantified as instructed (Verzicco *et al*., 20220).

CXCL-1, IL-1β, IL-6, and TNF-α serum concentrations: To assess serum concentrations of pro/anti-inflammatory cytokines, commercial ELISA kits sourced from RandD Systems, Inc. were employed following the manufacturer's guidelines. Initially, 50 µL of assay diluent RD1-54 was dispensed into the wells of a 96-well plate, followed by adding 50 µL of standard, control, or sample into respective wells. Subsequent to a 2-hour incubation period at room temperature, 100 µL of rat IL-6 conjugate was introduced into each well, followed by adding 100 µL of substrate solution to the mixture. After further incubation at ambient temperature for 30 minutes, 100 µL of stop solution was added to each well, and the resulting mixture was allowed to stand for an additional 30 minutes. The resultant solution's absorbance was assessed at 540 nm by a UV-visible spectrophotometer (V-630 Bio; JASCO, US) (Wang *et al*., 2021a).

Glutathione peroxidase (GPx), superoxide dismutase (SOD), and catalase (CAT) serum activity: To measure GPx activity, a Cell Signal ELISA kit obtained from a commercial supplier was utilized, following the manufacturer's instructions. Initially, 100 µl of lysis buffer was added to each serum sample in a 96-well plate, followed by a 10-minute incubation at 4°C. Subsequently, the mixture underwent centrifugation at 10,000 g for 5 minutes at 4°C, and the obtained supernatant was transferred to a fresh 96-well plate. Next, 50 µl of the working solution and 50 µl of the assay buffer from the kit were added to the wells. After incubation for 10 minutes at 37°C and further centrifugation at 10,000 g for 10 minutes at 37°C, the absorbance was measured at 450 nm using a JASCO V-630 Bio UV-visible spectrophotometer (US) (Wang *et al*., 2023).

For the assessment of SOD activity, a commercial Elabscience ELISA kit was employed, following the provided instructions. Initially, 50 µl of both the standard solution and the serum sample were transferred to the wells of a 96-well plate. Subsequently, 50 µl of primary antibody and 100 µl of conjugated horseradish peroxidase (HRP) were added to the respective wells. The mixture underwent incubation at 37°C for 30 minutes, followed by the addition of 50 µl of the stop solution and 90 µl of the substrate solution to the wells. After another 15-minute incubation at 37°C, the absorbance was measured at 450 nm using a JASCO V-630 Bio UV-visible spectrophotometer (US) (Wang *et al*., 2021a).

For the CAT activity assessment, a commercial Elabscience ELISA kit was employed, following the provided instructions. Initially, 100 µl of the standard solution and 100 µl of the serum sample were added to the wells of a 96-well plate and incubated for 2 hours at 25°C with gentle shaking. Subsequently, 100 µl of 1X

biotinylated antibody was added to the wells, followed by a 1-hour incubation at 25°C with gentle shaking. Next, 100 µl of the obtained streptavidin solution was transferred to the wells and incubated for 45 minutes at 25°C. Finally, TMB substrate reagent (100 µl) was added to the wells, and after a 30-minute incubation in a dark area at 25°C, the absorbance was measured at 450 nm using a JASCO V-630 Bio UV-visible spectrophotometer (US) (Wang *et al*., 2023).

Serum levels of nitric oxide (NO): The ZellBio ELISA kit was utilized to quantify serum levels of NO, serving as an indicator of free radical production, following the manufacturer's instructions. In accordance with the kit's protocol, 50 µl of serum and standard samples (diluted in assay buffer) were dispensed into the wells of a 96-well plate, followed by adding 10 µl of nitric reductase solution to each well. Following an incubation period of 20 minutes at 37°C, 25 µl of kit solutions B and A were transferred to the wells, followed by another incubation for 20 minutes at 37°C. Subsequently, the absorbance of the mixture was measured at 540 nm and 570 nm using a JASCO V-630 Bio UV-visible spectrophotometer (US) (Papageorgoulis *et al*., 2020).

Intestine total antioxidant capacity: One approach to assess total antioxidant capacity involves the ferric-reducing ability of plasma (FRAP) assay. Essentially, 100 mg of tissue, homogenized at 4°C, was initially combined with cold PBS (200 µl). Subsequently, 100 µl of this mixture was added to 10 µl of FRAP solution. Following incubation of the extract mixture for 15 minutes at 25°C and subsequent centrifugation at 12,000 g for 10 minutes, the resulting supernatant's absorbance was measured at 593 nm using a JASCO V-630 Bio UV-visible spectrophotometer (US) (Amjadi *et al*., 2020).

Intestine lipid peroxidation levels: One method to quantify the extent of lipid peroxidation involves measuring tissue thiobarbituric acid reactive substances (TBARS) levels. Initially, 100 µl of the homogenized tissue mixture from the intestine was combined with TBARS solution (100 µl). Following incubation for 30 minutes at 37°C and subsequent centrifugation at 12,000 g for 5 minutes, the resulting supernatant's absorbance was measured at 593 nm using a JASCO V-630 Bio UV-visible spectrophotometer (US) (Mosbah *et al*., 2018).

Intestine thiol levels: In order to assess tissue thiol levels, a significant indicator of tissue antioxidant capacity, 100 µl of the homogenized tissue mixture from the intestine was combined with 5,5-dithio-bis-(2-nitrobenzoic acid) (DTNB; 20 µl). Following an incubation period of 15 minutes at 37°C and subsequent centrifugation at 12,000 g for 5 minutes, the absorbance of the resulting supernatant was measured at 412 nm using a UV-visible spectrophotometer (Model No. V-630 Bio; JASCO, US) (Liu and O'Flaherty, 2017).

Intestine total RNA extraction: The Canvas Biotech Total RNA Purification Kit was utilized for total RNA extraction following the kit's instructions. Initially, 50 mg of intestine tissue was crushed, and then 300 µl of Buffer BLY was incubated with 10 µl of β-mercaptoethanol for 15 minutes at 4°C. Following centrifugation at 10,000 g for 2 minutes, the resulting mixture was transferred to a filter column, and after another round of centrifugation at 10,000 g for 2 minutes, 300 microliters of 70% ethanol were added and centrifuged once more at 10,000 g for 2 minutes. Subsequently, deionized water (50 µl) was added to the resulting pellet, which was then kept at -70°C. The RNA concentration was evaluated using a Nanodrop (Thermo Scientific spectrophotometer), while the quality of the extracted RNA was determined through 2% agarose gel electrophoresis (Wang *et al*., 2021b).

Bax, AQP3, p53, Caspase-3, AQP8, Bcl-2, and AQP10 genes expression with quantitative Real-Time PCR (qPCR): The qScriber cDNA synthesis kit was utilized to prepare the cDNA template following the provided instructions. Specifically, the extracted RNA (1 µg) was combined with 10 µl of qScriber reaction master mix, 8 µl of deionized water, and 1 µl of oligo and random hexamer primers. The resulting mixture underwent a temperature cycling program comprising 20 minutes at 55°C, followed by 5 minutes at 99°C, and finally 10 minutes at 30°C. Primer design was accomplished using Primer-3 software and Gene Runner version 6.5.52, while the designed primers were further validated using the NCBI database (https://www.ncbi.nlm.nih.gov/tools/primer-blast/). The β-actin gene was considered the internal reference, against which the expression of other genes was measured relative to.

For qPCR, the reaction mixture consisted of SYBR Green Master Mix (10 µl), cDNA (1 µl), and reverse/forward primers (1 µl) for each gene of interest. A total of 42 standard temperature cycles were employed, including annealing at 62°C for 1 minute, denaturation at 95°C for 5 minutes, and extension at 72°C for 2 minutes. Subsequently, the threshold cycle (CT) values of Bax, AQP3, p53, Caspase-3, AQP8, Bcl-2, and AQP10 were recorded, and the fold change formula was applied to calculate the relative expression of genes, considering the ΔΔCt method.

The fold formula change = $2^{-\Delta\Delta CT}$; ΔΔCt = [(Ct sample - Ct housekeeping gene) - (Ct sample – Ct control)] (Guo *et al*., 2018).

Bax, AQP3, p53, Caspase-3, AQP8, Bcl-2, and AQP10 proteins expression with western blotting: To assess the protein expression levels of AQP3, AQP10, and AQP8, Western blot analysis was conducted. Initially, a homogenized intestine tissue sample was prepared, and 100 mg of this sample was mixed with PBS (50 µl) and radio-immunoprecipitation assay buffer (100 µl).

Following centrifugation, 20 µl of loading buffer was added to a polyvinylidene fluoride (PVDF) membrane containing primary antibodies sourced from Cambridge Bioscience, UK, targeting AQP10 (Cat. No. HPA062621; 1:200), AQP3 (Cat. No. RC201856; 1:200), and AQP8 (Cat. No. HPA046259; 1:200). The mixture, along with an SDS polyacrylamide gel (10%), underwent separation using appropriate techniques. After a 12-hour incubation at 4°C, the membrane was subjected to further incubation with an HRP-conjugated secondary antibody for 40 minutes at 37°C. Subsequently, the signals emitted by the protein bands were captured and analyzed by Bio-Rad software, with the aid of an enhanced chemiluminescence reagent (e-BLOT Co., China). Further analysis was performed using Image J software (Zhao *et al*., 2017).

Intestine histopathology: To assess the degree of tissue damage and histopathological alterations in the intestine among different experimental groups, intestinal tissue samples were extracted and fixed in 10% formalin. Subsequently, tissue slices with a thickness of 5 micrometers were prepared following the standard tissue processing protocol. These slices were then subjected to staining with hematoxylin and eosin. Evaluation of intestinal morphology, including intestinal villi, intestinal glands, lymphocyte infiltration levels, villus height, and villus structure, was conducted using an optical microscope (Model No. BX61TRF; Olympus, Japan) coupled with the Moticam 1080N BMH camera system. Observations were made at a magnification of 100X (Wang *et al*., 2021b).

Statistical analyses: To compare the quantitative outcomes among the groups, one-way analysis of variance (ANOVA) followed by the Newman-Keuls post hoc test was employed at a significance level of $p < 0.05$. The normality and homogeneity of the data were assessed using the Kolmogorov-Smirnov test, where a p-value exceeding 0.05 indicated normal distribution and uniformity across groups. All findings are presented as mean ± standard deviation (SD). Data analysis was conducted using SPSS 16, while GraphPad Prism 9 software was utilized for graphical visualization.

RESULTS

LD_{50} of LDHE: Following a 24-hour observation of the groups subjected to LDHE treatment, the findings indicated that the established safe dosage (D safe) was identified as 2500 mg/kg, whereas the determined toxic dosage (D toxic) was 5000 mg/kg of LDHE. Utilizing Lork's formula, the calculated LD_{50} for LDHE was determined to be 3535 mg/kg. Consequently, this implies that doses lower than the LD_{50} of LDHE can be administered in animal studies.

Body weight and rat survival rate: Upon completion of the study, it was observed that CT treatment resulted in a significant ($p < 0.05$) reduction in the rats' weight compared to the healthy group. Moreover, the survival rate of rats in the CT group showed a noteworthy ($p < 0.05$) decrease compared to the healthy group. Conversely, in the CT+200 and 400 mg/kg LDHE groups, LDHE administration demonstrated a dose-dependent effect, eliciting a significant ($p < 0.05$) increase in rat weight compared to the CT group. Additionally, the survival rate of rats in the LDHE groups exhibited a substantial ($p < 0.05$) improvement compared to the CT group (Figure 1a and 1b).

Serum levels of ADH and AVP; The analysis of serum ADH and AVP data revealed a significant decrease ($p < 0.05$) in both indicators within the CT group compared to the healthy group. However, it's noteworthy that LDHE showed a dose-dependent response in increasing these serum parameters compared to the CT group. Interestingly, a significant ($p < 0.05$) increase in ADH serum levels was particularly evident in the CT+400 mg/kg LDHE group (Figure 2a).

Serum levels of IL-6, CXCL-1, TNF-α, and IL-1β: Through the induction of inflammatory responses, CT elevated pro-inflammatory cytokine levels and suppressed systemic anti-inflammatory cytokines. This resulted in a significant ($p < 0.05$) increase in the serum levels of all three pro-inflammatory cytokines (IL-6, TNF-α, and IL-1β) compared to the healthy group, accompanied by a noteworthy decrease in CXCL-1 levels. However, the study findings underscored the potent anti-inflammatory effects of LDHE. LDHE elevated the serum CXCL-1 level dose-dependently while concurrently reducing the levels of IL-6, TNF-α, and IL-1β pro-inflammatory cytokines compared to the CT group. These alterations were particularly significant ($p < 0.05$) in the 400 mg/kg dose (in the CT+400 mg/kg LDHE group) compared to the CT group (Figure 2b).

NO serum levels, along with CAT, GPx, and SOD serum activity: CT, by instigating the generation of free radicals, led to a noteworthy elevation in the serum level of NO compared to the healthy group. Conversely, LDHE exhibited a dose-dependent reduction in its levels relative to the CT group. This reduction reached significance ($p < 0.05$) at the dose of 400 mg/kg (in the CT+400 mg/kg LDHE group). Furthermore, CT significantly diminished the serum activity of all three antioxidant enzymes compared to the healthy group. Conversely, LDHE dose-dependently augmented the serum levels of these enzymes compared to the CT group, with a significant ($p < 0.05$) elevation observed at 400 mg/kg (in the CT+400 mg/kg LDHE group) compared to the CT group (Figure 3a).

TBARS, thiol, and FRAP levels in the intestine: TBARS, thiol, and FRAP levels, representing indicators of both total antioxidant capacity and lipid peroxidation, were evaluated as part of the study. The outcomes revealed that CT significantly ($p < 0.05$) diminished the tissue levels of all three factors compared to the healthy group. In contrast, LDHE, owing to its rich antioxidant content, demonstrated a dose-dependent ability to elevate the levels of these three factors compared to the CT group. This elevation reached significance ($p < 0.05$) at 400 mg/kg (in the CT+400 mg/kg LDHE group), marking the most substantial change compared to the CT group (Figure 3b).

Expression of intestine AQP3, AQP8, AQP10, Cas-3, Bcl-2, Bax, and p53 genes: A marked increase ($p < 0.05$) in the expression levels of pro-apoptotic genes Cas-3, Bax, and p53 was observed in the CT group compared to the healthy group. Concurrently, a significant decrease ($p < 0.05$) was detected in the expression of the anti-apoptotic gene Bcl-2. However, LDHE exhibited a mitigating effect on these changes by reducing the expression of Cas-3, Bax, and p53 genes and enhancing the expression of the anti-apoptotic Bcl-2 gene, thus inhibiting apoptotic cell processes. These alterations were particularly notable ($p < 0.05$) at the 400 mg/kg dose (in the CT+ 400 mg/kg LDHE group) compared to the CT group (Figure 4a).

One of the primary factors contributing to osmotic balance disruption in patients undergoing CT is the impairment of AQP functionality. The study revealed a significant reduction ($p < 0.05$) in the gene expression of all three AQPs (AQP3, AQP8, and AQP10) in the CT group compared to the healthy group. Conversely, LDHE exhibited the capacity to effectively upregulate the expression of all three AQP genes at a dosage of 400 mg/kg (in the CT+ 400 mg/kg LDHE group), a change found to be statistically significant ($p < 0.05$) compared to the CT group (Figure 4b).

Expression of intestine AQP3, AQP8, and AQP10 proteins: To further evaluate the impact of CT on the expression of AQP proteins in the intestine, we examined the protein levels of AQP3, AQP8, and AQP10. The results of this investigation revealed a significant decrease ($p < 0.05$) in the protein expression of all three AQPs in the CT group compared to the healthy group. However, in the CT+400 mg/kg LDHE group, there was a significant increase ($p < 0.05$) in the expression of all three AQP proteins relative to the CT group. This notable elevation was particularly prominent at a dosage of 400 mg/kg of LDHE and demonstrated statistical significance ($p < 0.05$) (Figure 5).

Intestine histopathological evaluations: The histopathological examination of the intestine across various groups revealed significant tissue damage induced by CT. This damage was characterized by the separation of the mucosa from the lamina propria and submucosa, disrupting the arrangement of intestinal villi. The underlying tissue showed signs of edema and inflammation. Additionally, the intestinal lumen exhibited uprooted villi and detached epithelial cells, indicating degradation of the basal and epithelial membranes, with apoptotic bodies present within the lumen.

Conversely, in the LDHE-treated groups, the integrity of intestinal villi was notably preserved, with this effect being dose-dependent. There was a significant reduction in tissue edema and lymphocyte infiltration. Moreover, groups receiving LDHE exhibited a normal architecture of absorptive epithelium (enterocytes) adjacent to a thin lamina propria and a submucosa rich in glands and vessels. This highlights the protective role of LDHE in maintaining the structural integrity of the intestine (Figure 6).

Table 1. Primer sequences

Gene	Sequences (5′–3′)	
AQP3	Forward: GTGACAGGAAGAGCCAGGAG	Reverse: CGCCCCTAGCAATACTACCA
Cas-3	Forward: CATTTCTTTAGTGATAAAA	Reverse: ATCATGGGATCTGTTTCTTT
AQP8	Forward: GGAGCTGCCATGTCAAAGAT	Reverse: CAGCCAGGAGAAATCAAACAGAGG
Bax	Forward: TGCCACTCAGAAGACTGTGG	Reverse: GGATGCAGGGATGTTCT
AQP10	Forward: GGTGTTGGTGATCGGAGTCT	Reverse: CGCCCTAAACACCTCATCC
β-actin	Forward: AGGCATCCTCACCCTGAAGTA	Reverse: CACACGCAGCTCATTGTAGA
Bcl-2	Forward: TTGCTACAGGGTTTCATCCA	Reverse: GAGTACCTGAACCGGCATCT
p53	Forward: GGTGTTGGTGATCGGAGTCT	Reverse: TTGCAGAGTGGAGGAAATGG

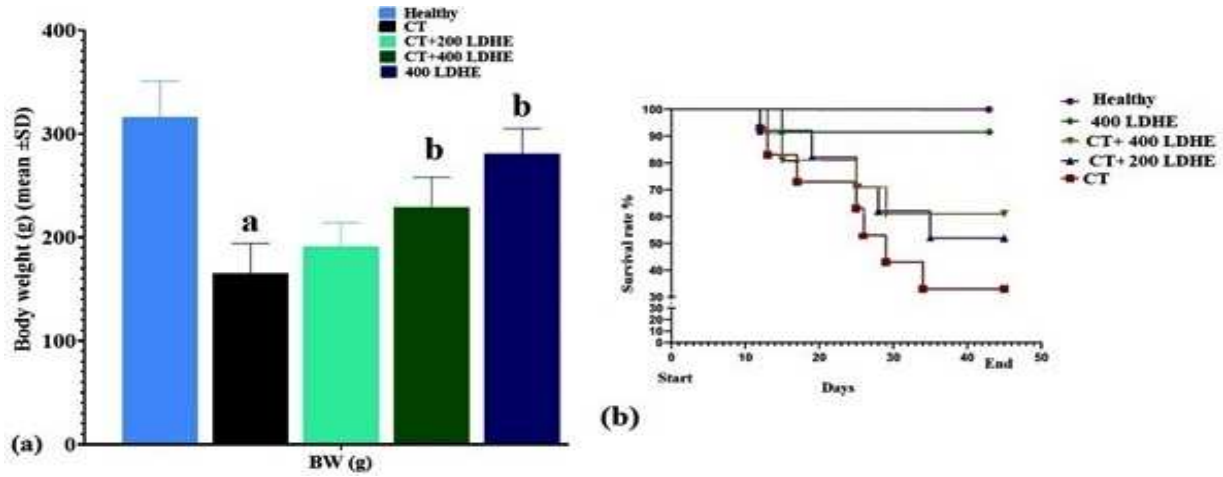

Figure 1: (a) Rats body (g) weight (means ± SD**; n=10/group) and (b) Kaplan-Meier survival curve in experimental groups. [a] (p<0.05) CT** vs. **healthy groups; [b] (p<0.05) LDHE + CT vs. CT groups.**

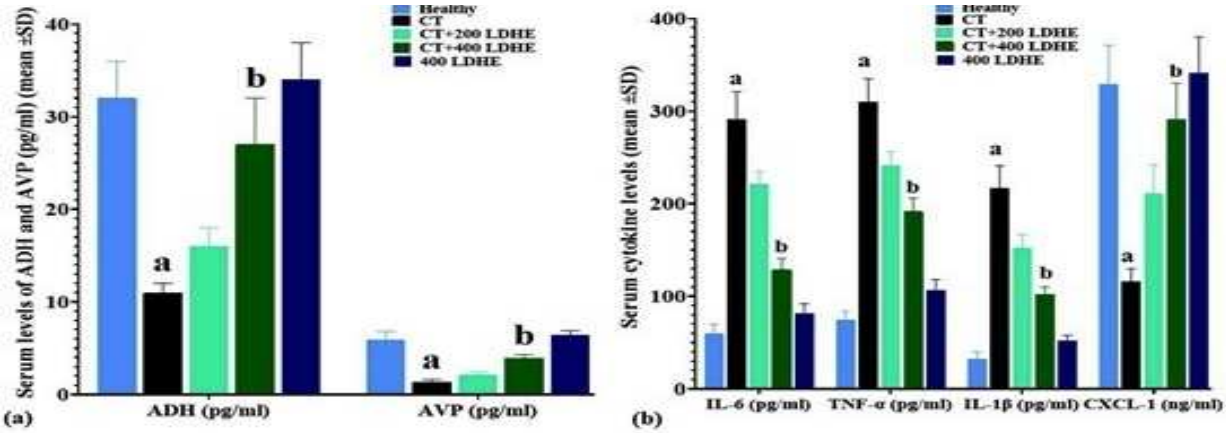

Figure 2: (a) Serum levels of ADH and AVP (pg/dl**) (b) Serum levels of IL-6, IL-1β,** TNF-α **(**pg/ml**),** and **CXCL-1 (**ng/ml**) (**means ± SD**; n=10/group) in experimental groups. [a] (p<0.05) CT** vs. **healthy groups; [b] (p<0.05) LDHE + CT vs. CT groups.**

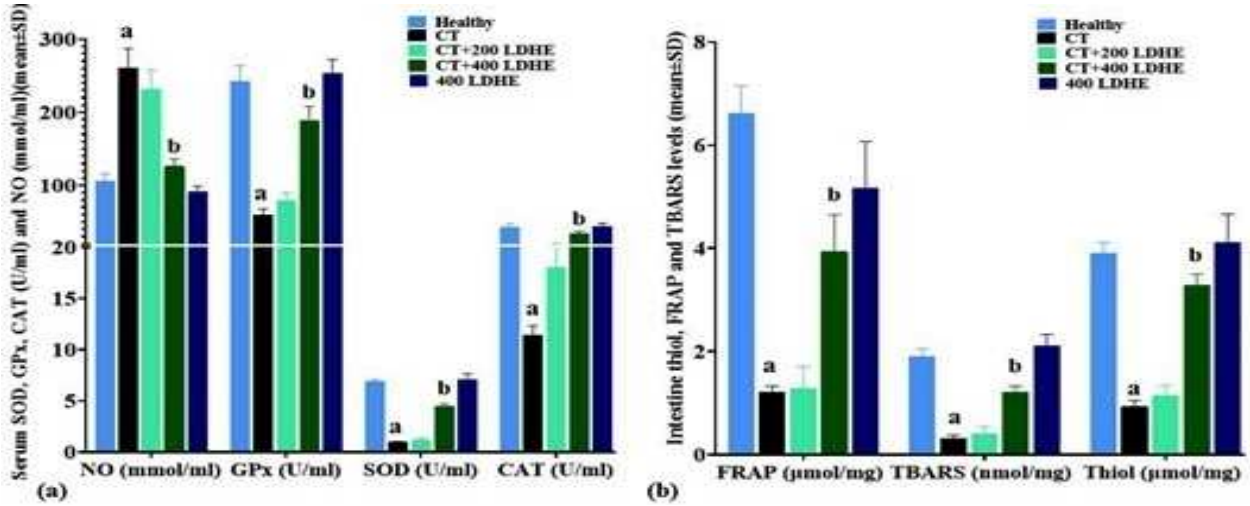

Figure 3: (a) Serum levels of NO (mmol/ml), alongside **the mean serum activity of SOD, CAT, and** GPx (U/ml) and **(b) intestine tissue levels of** TBARS (nmol/mg) **and** FRAP (µmol/mg) **(**means ± SD**; n=10/group) in experimental groups. [a] (p<0.05) CT** vs. **healthy groups; [b] (p<0.05) LDHE + CT vs. CT groups.**

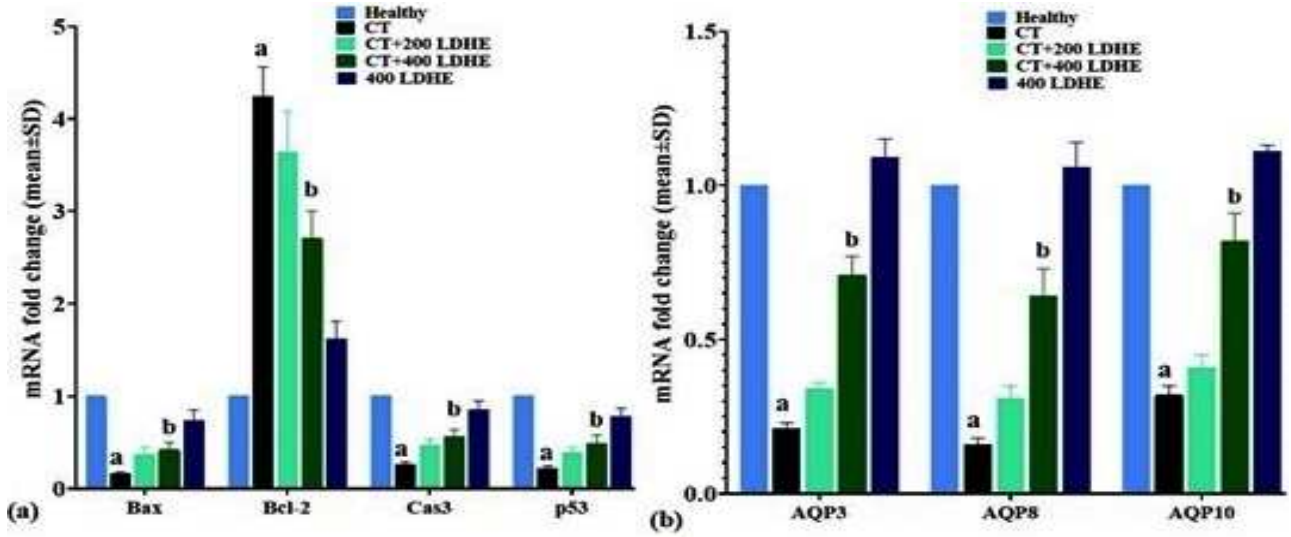

Figure 4: (a) Bax, Bcl-2, p53, and Cas-3 and (b) AQP3, AQP8, and AQP10 genes expression in intestine (means ± SD**; n=10/group) in experimental groups. [a] (p<0.05) CT** vs. **healthy groups; [b] (p<0.05) LDHE + CT vs. CT groups.**

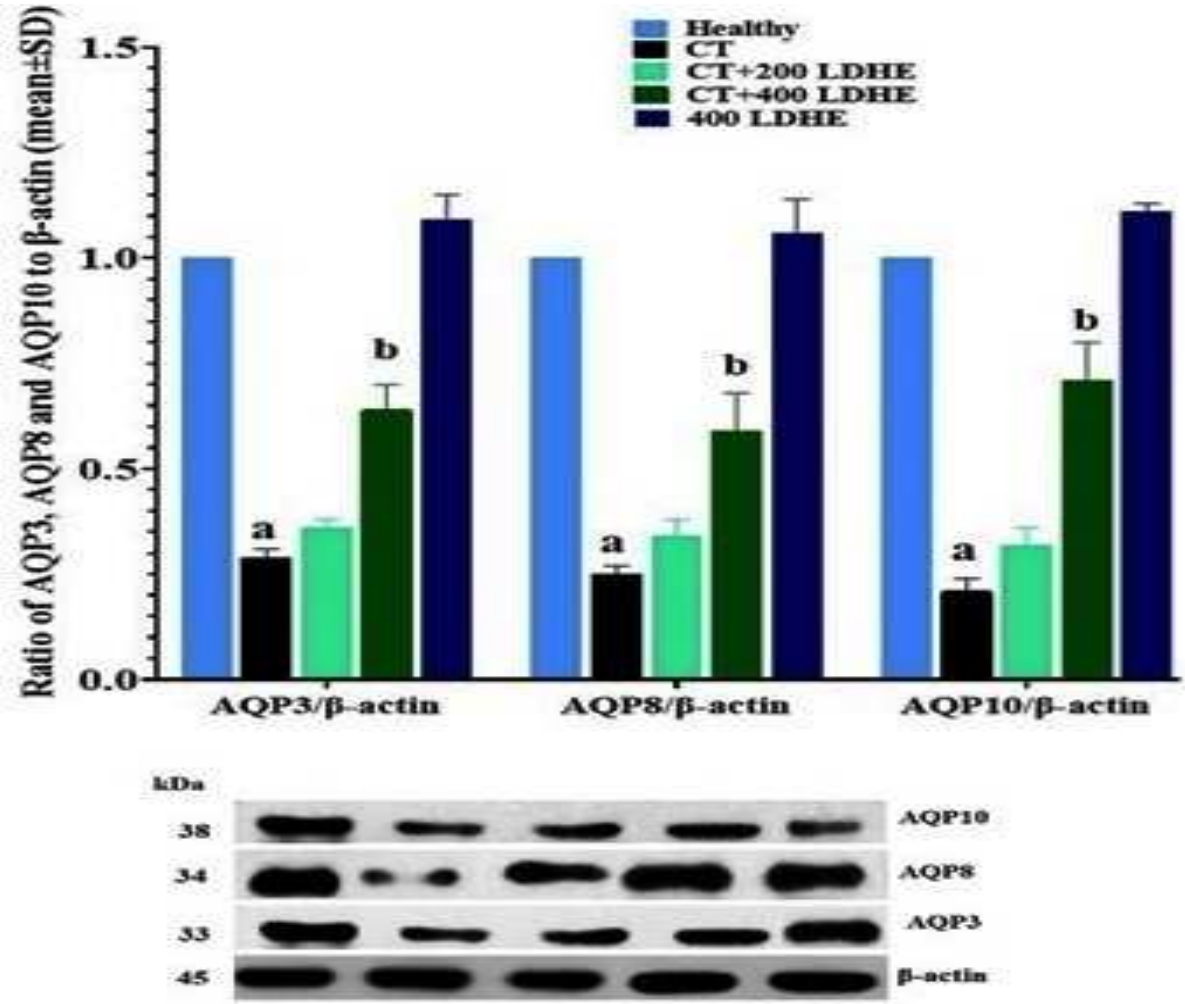

Figure 5: AQP3, AQP8, and AQP10 proteins expression in intestine (means ± SD**; n=10/group) in experimental groups. [a] (p<0.05) CT** vs. **healthy groups; [b] (p<0.05) LDHE + CT vs. CT groups.**

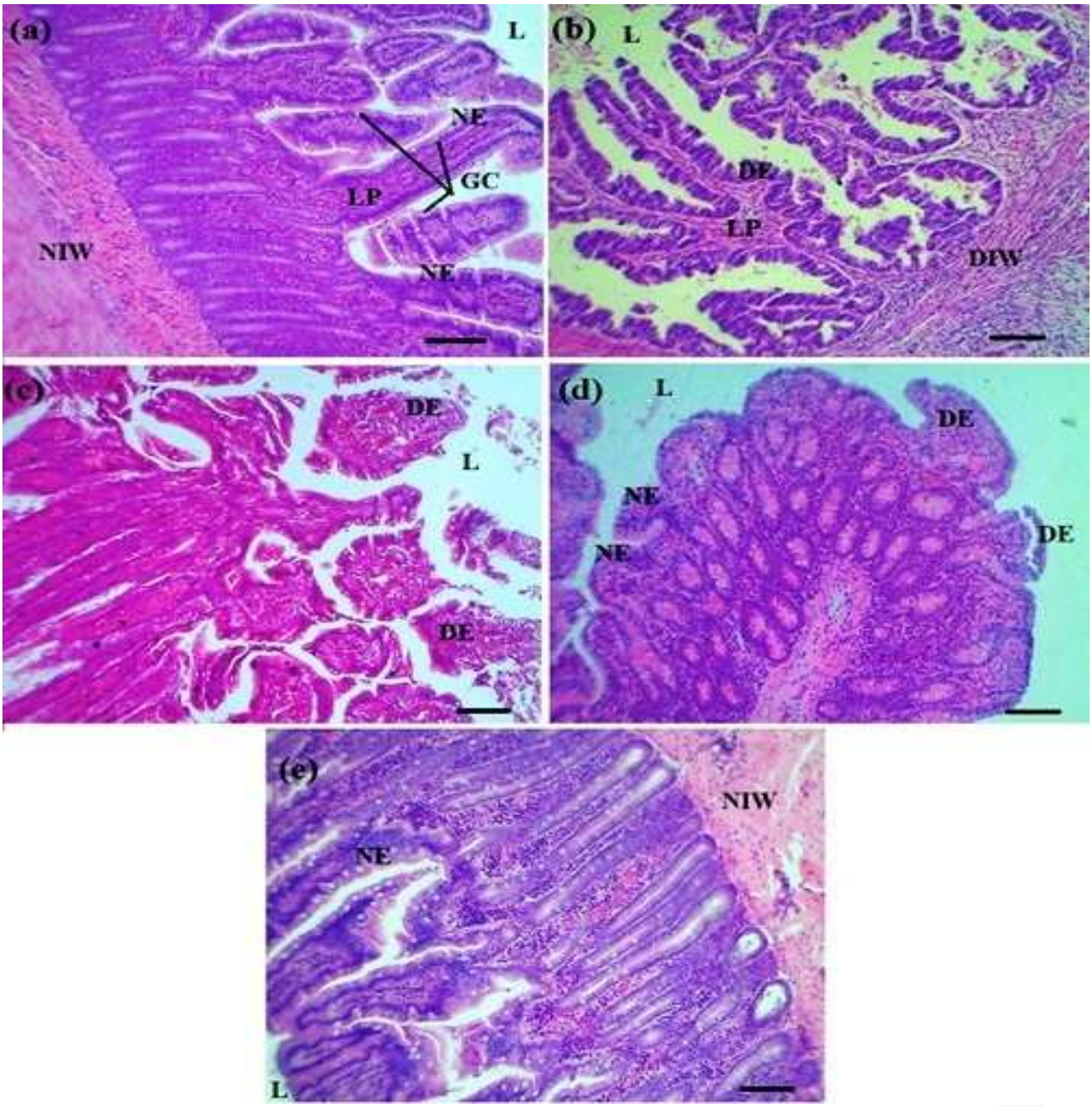

Figure 6: Evaluation of intestinal histopathology in healthy (a), CT (b1), CT+200 (c) and 400 (d) LDHE **and** 400 LDHE (e) (**HandE staining; × 100 with Scale bar = 200 µm). Goblet cell (GC), lamina propria (LP), lumen (L), normal epithelium (NE), degenerated epithelium (DE), normal intestinal wall (NIW), and degenerated intestinal wall (DIW).**

DISCUSSION

CT induced enterocolitis: The findings of this study reveal that CT and its metabolites induce enterocolitis in recipients through distinct mechanisms. CT, akin to certain other chemotherapy drugs, has the potential to impact the secretion of ADH and AVP through various molecular pathways. Previous animal studies have unveiled that specific chemotherapeutic agents, including cyclophosphamide and 5-FU, can disrupt the regulation of ADH and AVP release, resulting in fluid balance and electrolyte abnormalities (Sobol *et al*., 2023). Chemotherapy-induced nausea and vomiting (CINV) may trigger dysregulation of ADH and AVP secretion, leading to fluid retention and hyponatremia, particularly

with highly emetogenic chemotherapy regimens. Additionally, chemotherapy-induced mucositis and gastrointestinal disturbances can indirectly influence fluid intake and absorption, thereby impacting ADH and AVP regulation (Huang *et al*., 2022). This study demonstrated that CT caused dysregulation of ADH and AVP secretion, resulting in decreased serum levels by the study's end. Numerous studies have shown that 5-FU can generate ROS and free radicals, such as superoxide anions and hydroxyl radicals, inducing oxidative stress and damaging cellular components, such as proteins, DNA, and lipids (Aarnoutse *et al*., 2022). CT can activate various signaling pathways by releasing free radicals, including nuclear factor kappa B (NF-κB), MAPKs, the p53 pathway, and the phosphatidylinositol 3-kinase (PI3K)/Akt pathway (Gu *et al*., 2021; Terranova-Barberio *et al*., 2017). Moreover, CT inhibits the proliferation of normal cells through the NF-κB/p53/Cas-3 and WNT/β-catenin pathways while enhancing endogenous apoptotic pathways (Almaimani *et al*., 2022). Additionally, 5-FU functions as an antimetabolite by inhibiting thymidylate synthase, a crucial enzyme for DNA synthesis. This interference with DNA replication disrupts the cell cycle progression of enterocytes, inducing cell cycle arrest specifically in the G1 phase (Xiang *et al*., 2020). In a randomized clinical trial on colorectal cancer, chemotherapy using CT led to severe diarrhea, disrupting the balance of water and electrolytes, and impacting patients' overall well-being and treatment outcomes (Österlund *et al*., 2007). Furthermore, studies have investigated the effects of CT in rats, revealing that this chemotherapy drug hindered the activity of endogenous antioxidant enzymes such as GPx, CAT, and SOD, leading to intestinal mucosal damage and disrupted fluid accumulation and electrolyte secretion (Rtibi *et al*., 2018). In this study, CT treatment resulted in a decrease in total antioxidant capacity, as indicated by reduced levels of intestinal FRAP, TBARS, and total thiol. This decrease was attributed to the generation of free radicals, specifically an increase in NO levels. Moreover, CT treatment enhanced the activation of the mitochondrial apoptotic pathway, demonstrated by an upregulation of Bax, p53, and Caspase-3 gene expression in rats. These effects were accompanied by the inhibition of antioxidant enzyme activity, including GPx, CAT, and SOD. Patients undergoing CT treatment experienced significant adverse effects, including severe diarrhea and injuries to the gastrointestinal tract such as mucositis, enterocolitis, and, although rare, ileitis (Klimko *et al*., 2021). These complications have been found to disrupt the efficacy of CT in tumor treatment. Proposed strategies to manage diarrhea and restore electrolyte balance in patients receiving CT include the potential use of supplements or medications (Alzahrani *et al*., 2023). Another mechanism contributing to the onset of diarrhea following CT treatment is the mitotic arrest of crypt cells in the G2 phase. Recent research has highlighted abnormalities in goblet cells associated with CT usage, warranting further investigation (Almaimani *et al*., 2022). Among the various mechanisms impacted by CT, a notable aspect is the dysfunction, expression, and repair of AQPs, with a particular focus on AQP3 (Huang *et al*., 2022). Previous studies have demonstrated that this chemotherapy drug not only inhibits the expression of AQP3 but also induces apoptosis in enterocyte cells by enhancing the p53-dependent apoptotic pathway. Consistent with prior research, our present study similarly found that CT suppresses the expression of all three AQPs (AQP3, AQP8, and AQP10) present in intestinal cells (Trigueros-Motos *et al*., 2012).

LDHE ameliorates enterocolitis induced by CT: The current investigation highlights the dose-dependent mitigating impact of LDHE on CT-induced enterocolitis, particularly evident at a dosage of 400 mg/kg. This effect is orchestrated through diverse mechanisms. LDHE harbors numerous polyphenolic compounds, notably flavonoids, which exert multifaceted effects. These compounds not only synergistically enhance the efficacy of chemotherapy drugs in suppressing tumor cells but also shield parenchymal cells against oxidative, inflammatory, and apoptotic damage inflicted by chemotherapy agents. A study by Feng *et al*. (2022) illustrated the protective effects of LDHE extract on the liver and kidney against oxymetholone toxicity. The extract elevated the activity of glutathione reductase (GSR), SOD, CAT, peroxidase (POD), and Glutathione-S-transferase (GST), while augmenting the total antioxidant capacity and reducing tissue TBARS levels in the liver and kidney tissue. These combined effects preserved the physiological function and tissue structure of the liver in the face of oxymetholone toxicity. Numerous in vivo and in vitro studies have underscored the protective attributes of LDHE. Chyad (2017) explored the plant's protective effects against memory deficit, oxidative stress, and withdrawal syndrome caused by morphine. The plant extract significantly bolstered the brain's total antioxidant capacity, concurrently mitigating free radicals, and lipid peroxidation (malondialdehyde and NO production). Jamshidi Goharrizi *et al*. (2020) conducted an in vitro study on THP-1 cells, revealing the plant extract's immunomodulatory activity by inhibiting TNF-α and IL-12 pro-inflammatory cytokines. These anti-inflammatory effects were ascribed to phytyl linolenate, phytyl stearate, and phytyl docosanoate present in the plant. Additionally, Zinhari *et al*. (2017) and Cruz-Muñoz *et al*. (2022) reported that compounds derived from LDHE can suppress the growth of various cancer cell lines, including MCF-7 (breast ductal carcinoma), SW742 (colorectal adenocarcinoma), PLC/PRF/5 (liver hepatoma), and A375 (melanoma cancer). This property complements the action of

chemotherapy drugs in inhibiting the growth of diverse tumors, thereby enhancing therapeutic outcomes. In the present study, LDHE effectively augmented total antioxidant capacity (FRAP, TBARS, and thiol) and the activity of SOD, GPX, and CAT antioxidant enzymes. Furthermore, it exhibited proficiency in diminishing tissue and systemic levels of free radicals (NO), concurrently alleviating inflammatory pathways, and the release of associated cytokines (IL-6, TNF-α, and IL-1β).

Conclusion: LDHE exhibits dose-dependent ameliorating effects on CT-induced enterocolitis through its polyphenol compounds, including flavonoids. These compounds possess antioxidant, anti-inflammatory, and anticancer effects, contributing to the protection of normal cells and the suppression of tumor growth. It appears that the commercial extract or isolated compounds from LDHE hold potential for use as a prodrug or supplement in cancer patients. Nonetheless, further investigations into its diverse effects and additional protective pathways in various human and animal models are warranted.

REFERENCES

Aarnoutse, R., J. Ziemons J. de Vos-Geelen, L. Valkenburg-van Iersel, A. C. L. Wildeboer, A. Vievermans G. M. Creemers, A. Baars, ,H. J. H. M. J. Vestjens, G. N. Le, D. J. M. Barnett, S. S. Rensen, J. Penders and M. L. Smidt (2022). The role of intestinal microbiota in metastatic colorectal cancer patients treated with capecitabine. Clin. Colorectal Cancer. 21(2), e87–e97. doi: 10.1016/j.clcc.2021.10.004.

Ali, Q., R. Khalil, M. Nadeem, M. M. Azhar, M. M. Hafeez and A. Malik (2020). Antibacterial, antioxidant activities and association among plant growth related traits of Lepidium draba. Biol. Clin. Sci. Res., 2020(1). doi:10.54112/bcsrj.v2020i1.11.

Alzahrani, S. M., H. A. Al Doghaither, A. B. Al-Ghafari and P.N. Pushparaj (2023). 5-fluorouracil and capecitabine therapies for the treatment of colorectal cancer (Review). Onc. Rep., 50(4), 1–16. doi: 10.3892/or.2023.8612.

Almaimani, R. A., A. Aslam, J. Ahmad, M. Z. El-Readi, M. E. El-Boshy, A. H. Abdelghany, S. Idris, M. Alhadrami, M. Althubiti, H. A. Almasmoum, M. M. Ghaith, M. E. Elzubeir, S. Y. Eid and B. Refaat (2022). In vivo and in vitro enhanced tumoricidal effects of metformin, active vitamin D3, and 5-fluorouracil triple therapy against colon cancer by modulating the PI3K/Akt/PTEN/mTOR network. Cancers. 14(6), 1538. doi: 10.3390/cancers14061538.

Amjadi, A., H. Mirmiranpour, S. O. Sobhani and N. Moazami Goudarzi (2020). Intravenous laser wavelength radiation effect on LCAT, PON1, catalase, and FRAP in diabetic rats. Lasers Med. Sci., 35, 131-138. doi: 10.1007/s10103-019-02805-5.

Chyad, A (2017). Evaluation of anticancer, analgesic and anti-inflammatory activities of the ethanolic extract of Lepidium draba Linn. leaves. Adv. Anim. Vet. Sci., 5(1), 7-13. doi: 10.14737/journal.aavs/2017/5.1.7.13.

Cruz-Muñoz, J. R., T. Barrios-García, E. E. Valdez-Morales, M. F. Durán-Vazquez, K. B. Méndez-Rodríguez, A. Barajas-Espinosa and R. G. Alba (2022). Ethanolic extract from Lepidium virginicum L. ameliorates DNBS-induced colitis in rats. J. Ethnopharmacol., 289, 115056. doi:10.1016/j.jep.2022.115056.

Feng, J., H. Gao, L. Yang, Y. Xie, A. E. El-Kenawy and A. F. El-kott (2022). Renoprotective and hepatoprotective activity of Lepidium draba L. extracts on oxymetholone-induced oxidative stress in rat. J. Food Biochem., 46(9), e14250. doi: 10.1111/jfbc.14250.

Festing, M. F (2006). Design and statistical methods in studies using animal models of development. Ilar J., 47(1), 5-14. doi: 10.1093/ilar.47.1.5.

Inala, M. S. R. and K. Pamidimukkala (2023). Amalgamation of quercetin with anastrozole and capecitabine: A novel combination to treat breast and colon cancers–An in vitro study J. Cancer. Res. Ther., 19(Suppl 1), S93-S105. doi: 10.4103/jcrt.JCRT_599_20.

Gu Y., J. Zhu, Y. Xu, C. Wan and J. Qian (2021). Trial study of capecitabine metronomic chemotherapy combined with exemestane inhibit proliferation of breast cancer cells by PI3K-AKT signaling pathway. Cancer Res Clin. 6, 401–407.

Guo, S., X. W. Meng, X. S. Yang, X. F. Liu, C. H. Ou-Yang and C. Liu (2018). Curcumin administration suppresses collagen synthesis in the hearts of rats with experimental diabetes. Acta Pharmacol. Sin., 39(2), 195-204. doi: 10.5555/20183104984.

Huang, J., A. Y. M. Hwang, Y. Jia, B. Kim, M. Iskandar, A. I. Mohammed and N. Cirillo (2022). Experimental chemotherapy-induced mucositis: A scoping review guiding the design of suitable preclinical models. Int. J. Mol. Sci. 23(23), 15434. doi: 10.3390/ijms232315434.

Jamshidi Goharrizi, K., F. Fatehi, M. Nazari, F. Salehi and M. Maleki (2020). Assessment of changes in the content of sulforaphane and expression levels of CYP79F1 and myrosinase genes and proteomic profile of Lepidium draba plant under water-deficit stress induced by polyethylene

glycol. Acta Physiol. Plant., 42, 1-18. doi: 10.1007/s11738-020-03085-1.

Jelodar, G., S. Masoomi and F. Rahmanifar (2018). Hydroalcoholic extract of flaxseed improves polycystic ovary syndrome in a rat model. Iran. J. Basic Med. Sci., 21(6), 645. doi: 10.22038/IJBMS.2018.25778.6349.

Kamar, S. S., M. H. Baky and A. I. Omar (2020). The beneficial influence of rhubarb on 5-fluorouracil-induced ileal mucositis and the combined role of aquaporin-4, tumour necrosis factor-α, nuclear factor-kappa B and matrix metalloproteinase-9 in rat model: histological study. Anat. Cell Biol., 53(2), 228-239. doi: 10.5115/acb.20.014.

Klimko A., C. G. Tieranu, A. O. Olteanu, C. M. Preda, E. M. Ionescu and C. Tieranu (2021). Capecitabine-induced terminal ileitis: Case report and literature review. Cureus. 13(4), e14621. doi: 10.7759/cureus.1462.

Liu, Y. and C. O'Flaherty (2017). In vivo oxidative stress alters thiol redox status of peroxiredoxin 1 and 6 and impairs rat sperm quality. Asian J. Androl., 19(1), 73. doi: 10.4103/1008-682X.170863.

Masuda, N., S. J. Lee, S. Ohtani, Y. H. Im, E. S. Lee, I. Yokota and M. Toi (2017). Adjuvant capecitabine for breast cancer after preoperative chemotherapy. N. Engl. J. Med., 376(22), 2147-2159. doi: 10.1056/NEJMoa1612645.

McRee, A. J., P. K. Marcom, D. T. Moore, W. C. Zamboni, Z. A. Kornblum, Z. Hu and E. C. Dees (2018). A phase I trial of the PI3K inhibitor buparlisib combined with capecitabine in patients with metastatic breast cancer. Clin. Breast Cancer, 18(4), 289-297. doi:10.1016/j.clbc.2017.10.014.

Mosbah, R., Z. Djerrou and A. Mantovani (2018). Protective effect of Nigella sativa oil against acetamiprid induced reproductive toxicity in male rats. Drug Chem. Toxicol., 41(2), 206-212. doi:10.1080/01480545.2017.1337127.

Österlund P., T. Ruotsalainen, R. Korpela, M. axelin, A. Ollus, P. Valta, M. Kouri, I. Elomaa and H. Joensuu (2007). Lactobacillus supplementation for diarrhoea related to chemotherapy of colorectal cancer: A randomised study. Br. J. Cancer. 97(8), 1028–1034. doi: 10.1038/sj.bjc.6603990.

Ouissem, B. S., B. Sabrina, B. Lotfi, R. Khellaf, B. Chawki, D. Ibrahim and B. Fadila (2018). HPLC analysis and antioxidant properties of Algerian Lepidium draba ethyl acetate extract. J. Biol. Act. Prod. Nat., 8(4), 265-271. doi.org/10.1080/22311866.2018.1511381.

Papageorgoulis, A., P. Fallon, N. Mpalantes, D. Papageorgouli and N. Pitsikas (2020). Repeated but not acute exposure with a low dose range of the nitric oxide (NO) donor sodium nitroprusside (SNP) induces anxiolytic-like behaviour in a dose-independent manner in two different rat models of anxiety. Nitric Oxide, 99, 1-6. doi:10.1016/j.niox.2020.03.005.

Reyna-Figueroa, J., E. Barrón-Calvillo, C. García-Parra, P. Galindo-Delgado, C. Contreras-Ochoa, A. Lagunas-Martínez. and A. E. Limón-Rojas (2019). Probiotic supplementation decreases chemotherapy-induced gastrointestinal side effects in patients with acute leukemia. Pediatr. Hematol. Oncol. J., 41(6), 468-472. doi: 10.1097/MPH.0000000000001497.

Rtibi K., S. Selmi, D. Grami, M. Amri, H. Sebai and L. Marzouki (2018). Contribution of oxidative stress in acute intestinal mucositis induced by 5 fluorouracil (5-FU) and its pro-drug capecitabine in rats. Toxicol. Mech. Methods. 28(4), 262–267. doi: 10.1080/15376516.2017.1402976.

Sakai, S., S. Kobuchi, Y. Ito and T. Sakaeda, (2020). Assessment of pharmacokinetic variations of capecitabine after multiple administration in rats: a physiologically based pharmacokinetic model. Cancer Chemother Pharmacol., 85, 869-880. doi: 10.1007/s00280-020-04057-5.

Salaroglio, I. C., E. Mungo, E. Gazzano, J. Kopecka and C. Riganti (2019). ERK is a pivotal player of chemo-immune-resistance in cancer. Int. J. Mol. Sci., 20(10), 2505. doi:10.3390/ijms20102505

Shakir, F. T. Z., R. Sultan, R. Siddiqui, M. Z. Shah, A. Javed and J. Coll (2019). Adult necrotising enterocolitis in a breast cancer patient after first cycle of adjuvant chemotherapy. J. Coll. Physicians Surg. Pakistan, 29(10), 1006-8.

Siddiqui, N. S., A. Godara, M. M. Byrne and M. W. Saif (2019). Capecitabine for the treatment of pancreatic cancer. Expert Opin Pharmacother., 20(4), 399-409. doi:10.1080/14656566.2018.1560422.

Sobol N. T., L. M. Solerno, C. Llavona, D. F. Alonso and J. Garona J (2023). Vasopressin analog [V4Q5] dDAVP exerts cooperative anticancer effects in combination with low-dose 5-fluorouracil on aggressive colorectal cancer models. World J. Oncol. 14(6), 540–550. doi: 10.14740/wjon1715.

Terranova-Barberio M., B. Pecori, M. S. Roca, S. Imbimbo, F. Bruzzese, A. Leone, P. Muto, P. Delrio, A. Avallone, A. Budillon and E. Di Gennaro (2017). Synergistic antitumor interaction between valproic acid, capecitabine and radiotherapy in colorectal cancer: Critical role of p53. J. Exp. Clin. Cancer Res. 36(1), 177. doi: 10.1186/s13046-017-0647-5.

Tóth, Š., Jonecová, Z., K. Čurgali, M. Maretta, J. Šoltés, M. Švaňa and P. Kruzliak (2017). Quercetin attenuates the ischemia reperfusion induced COX-2 and MPO expression in the small intestine mucosa. Biomed. Pharmacother., 95, 346-354. doi:10.1016/j.biopha.2017.08.038.

Trigueros-Motos L., S. Pérez-Torras, F. J. Casado, M. Molina-Arcas and M. Pastor-Anglada (2012). Aquaporin 3 (AQP3) participates in the cytotoxic response to nucleoside-derived drugs. BMC Cancer. 12, 434. doi: 10.1186/1471-2407-12-434.

van den Boogaard, W. M., D. S. Komninos and W. P. Vermeij (2022). Chemotherapy side-effects: not all DNA damage is equal. Cancers, 14(3), 627. doi:10.3390/cancers14030627.

Verzicco, I., S. Tedeschi, G. Graiani, A. Bongrani, M. L. Carnevali, S. Dancelli and A. Cabassi (2022). Evidence for a Prehypertensive Water Dysregulation Affecting the Development of Hypertension: Results of Very Early Treatment of Vasopressin V1 and V2 Antagonism in Spontaneously Hypertensive Rats. Front. cardiovasc. Med., 9, 897244. doi:10.3389/fcvm.2022.897244.

Wang, Z., X. Jiang, L. Zhang and H. Chen (2023). Protective effects of Althaea officinalis L. extract against N-diethylnitrosamine-induced hepatocellular carcinoma in male Wistar rats through antioxidative, anti-inflammatory, mitochondrial apoptosis and PI3K/Akt/mTOR signaling pathways. Food Sci. Nutr., 11(8), 4756-4772. doi:10.1002/fsn3.3455.

Wang, Y., L. Bai, J. Zhang, H. Li, W. Yang and M. Li (2021). Lepidium draba L. leaves extract ameliorated cyclophosphamide-induced testicular toxicity by modulation of ROS-dependent Keap1/Nrf2/HO1, Bax/Bcl2/p53/caspase-3, and inflammatory signaling pathways. J. Food Biochem., 45(12), e13987. doi:10.1111/jfbc.13987.

Wang, L., R. Wang, G. Y. Wei, R. P. Zhang, Y. Zhu, Z. Wang and G. H. Du (2021). Cryptotanshinone alleviates chemotherapy-induced colitis in mice with colon cancer via regulating fecal-bacteria-related lipid metabolism. Pharmacol. Res., 163, 105232. doi:10.1016/j.phrs.2020.105232.

Wang, Y., X. Liu, J. Liu and T. Zhang (2019). Knockdown of REG Iα enhances the sensitivity to 5-fluorouracil of colorectal cancer cells via cyclin D1/CDK4 pathway and BAX/BCL-2 pathways. Cancer Biother. Radiopharm., 34(6), 362-370. doi: 10.1089/cbr.2018.2746.

Xiang D. C., J. Y. Yang, Y. J. Xu, S. Zhang, M. Li, C. Zhu, C. L. Zhang and D. Liu D (2020). Protective effect of andrographolide on 5-Fu induced intestinal mucositis by regulating p38 MAPK signaling pathway. Life Sci. 252, 117612. doi: 10.1016/j.lfs.2020.117612.

Zhao, L., Q. Gu, L. Xiang, X. Dong, H. Li, J. Ni and G. Chen (2017). Curcumin inhibits apoptosis by modulating Bax/Bcl-2 expression and alleviates oxidative stress in testes of streptozotocin-induced diabetic rats. Ther. Clin. Risk Manag., 1099-1105. doi: 10.2147/TCRM.S141738.

Zhao, G., J. Williams, M. K. Washington, Y. Yang, J. Long, S. D. Townsend and F. Yan (2022). 2'-Fucosyllactose ameliorates chemotherapy-induced intestinal mucositis by protecting intestinal epithelial cells against apoptosis. Cell. Mol. Gastroenterol. Hepatol., 13(2), 441-457. doi:10.1016/j.jcmgh.2021.09.015.

Zhu, J., W. Zeng, L. Ge, X. Yang, Q. Wang and H. Wang (2019). Capecitabine versus 5-fluorouracil in neoadjuvant chemoradiotherapy of locally advanced rectal cancer: A meta-analysis. Medicine, 98(17). doi: 10.1097/MD.0000000000015241.

Zhu, S., J. Ran, B. Yang and Z. Mei (2017). Aquaporins in digestive system. Aquaporins, 123-130. doi: 10.1007/978-94-024-1057-0_8.

Zinhari, Z., S. Pourseyedi and J. Zolalo (2017). A novel in vitro transformation of Lepidium draba L. using rapid direct shoot regeneration. 3 Biotech, 7, 1-13. doi:10.1007/s13205-017-0915-2.